

Critical behavior of lattice gauge theory Rydberg simulators from effective Hamiltonians

Jin Zhang¹, S.-W. Tsai², and Y. Meurice³

¹ *Department of Physics and Chongqing Key Laboratory for Strongly Coupled Physics, Chongqing University, Chongqing 401331, China*

² *Department of Physics and Astronomy, University of California, Riverside, CA 92521, USA and*

³ *Department of Physics and Astronomy, University of Iowa, Iowa City, IA 52242, USA*

(Dated: December 8, 2023)

Abstract

We consider multileg ladders of Rydberg atoms which have been proposed as quantum simulators for the compact Abelian Higgs model (CAHM) in 1+1 dimensions [Y. Meurice, Phys. Rev. D 104, 094513 (2021)] and modified versions of these simulators such as triangular prisms. Starting with the physical Hamiltonian for the analog simulator, we construct translation-invariant effective Hamiltonians by integrating over the simulator high-energy states produced by the blockade mechanism when some of the atoms are sufficiently close to each others. Remarkably, for all the simulators considered, the effective Hamiltonians have the three types of terms present for the CAHM (Electric field, matter charge and currents energies) but, in addition, terms quartic in the electric field. For the two leg ladder, these additional terms cannot be removed by fine-tuning the adjustable parameters of currently available devices. For positive detuning, the new terms create highly-degenerate vacua resulting in a very interesting phase diagram. Using numerical methods, we demonstrate the close correspondence between the physical simulator and the effective description for the ground state energy and real-time evolution. We discuss the phase diagram at fixed geometry with variable Rabi frequency and detuning and show that a rich variety of phases can be reached with potential interest in the context of QCD at finite density. We illustrate how the effective description can be used to design simulators with desirable properties from the point of view of constructing hybrid event generators.

I. INTRODUCTION

The idea of using quantum devices to study the real-time evolution of strongly interacting particles in high-energy and nuclear physics has gained considerable interest in recent years [1–4]. In this context, the possibility of building arrays of Rydberg atoms of significant size with adjustable geometry and external parameters [5–7] offer many new possibilities for analog simulations of lattice field theory models. In addition, publicly available interfaces [8, 9] allow users to configure arrays involving hundreds of Rydberg atoms and run their own experiments. This sets the path for extensive empirical exploration by scientists who don't have direct access to this type of facilities.

This new technology has been used to propose simulations of spin and lattice gauge theory models [10–15]. One of the simplest model is the Abelian Higgs model [13, 16–20]. In 1+1 dimensions, and after elimination of the non-compact Brout-Englert-Higgs mode, the Hamiltonian reads

$$\hat{H}_{CAHM} = \frac{U}{2} \sum_{i=1}^{N_s} (\hat{L}_i^z)^2 - Y \sum_{i=1}^{N_s-1} \hat{L}_i^z \hat{L}_{i+1}^z - X \sum_{i=1}^{N_s} \hat{U}_i^x \quad (1)$$

with N_s the number of sites, $\hat{L}^z|m\rangle = m|m\rangle$ and m a discrete electric field quantum number ($-\infty < m < +\infty$), and $\hat{U}^x \equiv \frac{1}{2}(\hat{U}^+ + \hat{U}^-)$ with $\hat{U}^\pm|m\rangle = |m \pm 1\rangle$. Note that in the derivation of the Hamiltonian we obtain a term of the form $\frac{Y}{2} \sum_i (\hat{L}_{i+1}^z - \hat{L}_i^z)^2$ that accounts for matter interactions, however for matching purposes which become clear later, we have reabsorbed the local quadratic couplings in the definition of the coupling U . In practice, we also apply truncations: for a spin- m_{max} truncation we have $\hat{U}^\pm|\pm m_{max}\rangle = 0$. In the following we focus on the spin-1 truncation.

It has been argued [13] that this spin-1 Hamiltonian can be approximately simulated using arrays of Rydberg atoms by adapting the optical lattice construction using ^{87}Rb atoms separated by controllable (but not too small) distances, coupled to the excited Rydberg state $|r\rangle$ with a detuning Δ . The ground state is denoted $|g\rangle$ and the two possible states $|g\rangle$ and $|r\rangle$ can be seen as a qubit with $n|g\rangle = 0$, $n|r\rangle = |r\rangle$. The Hamiltonian for a generic array reads

$$\hat{H} = \frac{\Omega}{2} \sum_i (|g_i\rangle\langle r_i| + |r_i\rangle\langle g_i|) - \Delta \sum_i \hat{n}_i + \sum_{i<j} V_{ij} \hat{n}_i \hat{n}_j, \quad (2)$$

where the indices label atoms and $V_{ij} = \Omega R_b^6 / r_{ij}^6$ for a distance r_{ij} between the atoms labelled as i and j . Note: when $r = R_b$, the Rydberg blockade radius within which states with two

or more Rydberg states have a low probability, we have $V = \Omega$. The simplest simulator is a two-leg ladder [13] with the correspondence:

$$|gg\rangle \rightarrow |m = 0\rangle, |gr\rangle \rightarrow |m = 1\rangle, |rg\rangle \rightarrow |m = -1\rangle, \quad (3)$$

for the two atoms on a rung. If the distance separating these two atoms is small enough, the state $|rr\rangle$ is unlikely to appear. In Ref. [13], it was shown that a perfect matching could be obtained for the individual sites, however, the nearest-neighbor (NN) interactions controlled by Y could not be matched exactly using the current technology where all the interactions are repulsive.

In this article, we show that it is possible to construct an effective Hamiltonian for the simulator provided that the set of atoms used to emulate the local spin-1 degrees of freedom are close enough, in other words, if the distance separating them is less than R_b . We will show that if these sets form the rungs of a ladder and if the distance between the next-nearest-neighbor (NNN) rungs is larger than R_b , the effective Hamiltonian has the three types of terms found in Eq. (1) with in addition a quartic term of the form $\sum_{i=1}^{N_s-1} (\hat{L}_i^z)^2 (\hat{L}_{i+1}^z)^2$. The ladder models considered and their effective Hamiltonians are presented in Sec. II. Numerical tests are performed in Sec. III. Their phase diagrams are discussed in Sec. IV. Practical applications involving systems that can be simulated at facilities such as QuEra are discussed in Sec. V.

II. RYDBERG SIMULATOR

The multileg ladder of Rydberg atoms is a promising quantum simulator for exotic quantum critical phenomena and lattice gauge theories, as we can use different rung geometries to encode various local degrees of freedom. Figure 1 shows a rectangular multileg ladder of Rydberg atoms with N_s rungs and N_l legs. The Hamiltonian of the multileg ladder reads

$$\begin{aligned} \hat{H}_{m\text{LR}} = & \frac{\Omega}{2} \sum_{\substack{i=1,2,\dots,N_s \\ s=1,2,\dots,N_l}} (|g_{i,s}\rangle\langle r_{i,s}| + h.c.) - \Delta \sum_{\substack{i=1,2,\dots,N_s \\ s=1,2,\dots,N_l}} \hat{n}_{i,s} \\ & + \sum_{(i,s) \neq (i',s')} V_{i,s;i',s'} \hat{n}_{i,s} \hat{n}_{i',s'}, \end{aligned} \quad (4)$$

where $|r_{i,s}\rangle (|g_{i,s}\rangle)$ is the Rydberg excited (ground) state at the site on the i th rung and the s th leg, $\hat{n}_{i,s} = |r_{i,s}\rangle\langle r_{i,s}|$ is the Rydberg number operator, Ω and Δ are the Rabi frequency

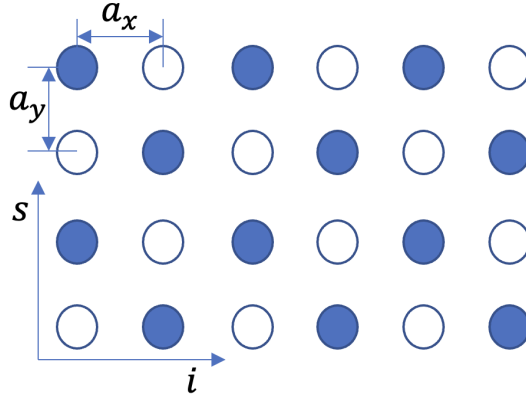


FIG. 1. The rectangular multileg ladder of Rydberg atoms, $a_{x(y)}$ is the lattice spacing in $x(y)$ directions, i labels rungs and s labels legs. Here it is a checkerboard stripe, where empty circles represent atomic ground state $|g\rangle$, and the blue solid circles are excited Rydberg states $|r\rangle$.

and detuning, respectively. The interaction between Rydberg states are long-range van der Waals repulsive interactions taking the form

$$\begin{aligned}
 V_{i,s;i',s'} &= \frac{C_6}{\left[(i-i')^2 a_x^2 + (s-s')^2 a_y^2 \right]^3} \\
 &= \frac{V_0}{\left[(i-i')^2 / \rho^2 + (s-s')^2 \right]^3}
 \end{aligned} \tag{5}$$

where a_x (a_y) is the lattice spacing in x (y) direction, C_6 is a constant, $V_0 = C_6/a_y^6$, and $\rho = a_y/a_x$ is the inverse aspect ratio. The Rydberg blockade mechanism means that at most one Rydberg state is allowed with a significant probability within a sufficiently small radius, typically the blockade radius R_b that is defined by equating the interaction energy at distance R_b to the Rabi frequency, $C_6/R_b^6 = \Omega$, thus $R_b = (C_6/\Omega)^{1/6}$. Below R_b , the interaction between Rydberg states is so strong that the laser field cannot excite two Rydberg states simultaneously [21]. This imposes restrictions on the low-energy excitations for those building blocks of quantum systems. The Rydberg system is highly programmable. In our case, both the geometry of rungs and the parameters can be tuned to encode local spin degrees of freedom, and realize a class of spin chains. In the following, we label the leg by the spin projection quantum numbers.

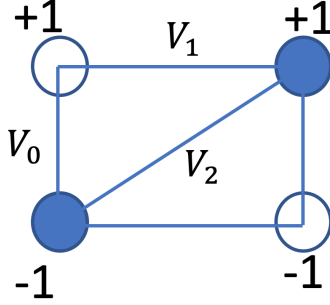


FIG. 2. The two-leg Rydberg ladder with $N_s = 2$ rungs. In each rung, the state with one Rydberg state in the upper leg is labeled by the spin $|+1\rangle$ state and the one with one Rydberg state in the lower leg is labeled by the spin $|-1\rangle$ state. The spin $|0\rangle$ state labels the state with no Rydberg state in the rung. The interactions between Rydberg states in the same rung, in the same leg, and in different legs are V_0 , V_1 , and V_2 , respectively.

A. Two-leg ladder

The one-dimensional Rydberg chain is a special case of the multi-leg ladder system with $N_l = 1$. For a two-leg ladder, $N_l = 2$, there are four degrees of freedom in each rung: $|g_{i,1}g_{i,2}\rangle$, $|g_{i,1}r_{i,2}\rangle$, $|r_{i,1}g_{i,2}\rangle$, and $|r_{i,1}r_{i,2}\rangle$. The corresponding on-rung energy is 0, $-\Delta$, $-\Delta$, and $V_0 - 2\Delta$, respectively. In principle, the four states can be used to represent the four projected states in z direction for spin-3/2, then the on-rung interaction can be expressed by $\sum_{n=1}^4 A_n (\hat{L}_i^z)^n$, where the coefficients A_n can be found by matching the energy spectrum. However, in real quantum systems, the most common onsite terms are the linear term that is coupled to the external field and the quadratic term that is the single-ion anisotropy. In addition, the Rydberg interaction is strong when the rung size is smaller than the Rydberg blockade radius such that the $|r_{i,1}r_{i,2}\rangle$ state is not likely to appear. Here we only consider a spin-1 realization by mapping the first three states to the spin-1 projected states $|0\rangle$, $|+1\rangle$, $|-1\rangle$, respectively. The onsite interaction term in spin language is thus $-\Delta (\hat{L}_i^z)^2$. The relation of the z -component spin operator to the Rydberg number operator is defined as [13]

$$\hat{L}_i^z = \hat{n}_{i,+1} - \hat{n}_{i,-1}.$$

If we take the square of this equation, use the property $\hat{n}^2 = \hat{n}$, and drop the term $\hat{n}_{i,+1}\hat{n}_{i,-1}$ which is zero in the low energy sector we obtain effectively

$$(\hat{L}_i^z)^2 = \hat{n}_{i,+1} + \hat{n}_{i,-1} \quad (6)$$

Solving for $\hat{n}_{i,m}$ we get

$$\hat{n}_{i,+1(-1)} = \left[\left(\hat{L}_i^z \right)^2 \pm \hat{L}_i^z \right] / 2. \quad (7)$$

Plugging Eq. 7 into the Rydberg interactions, we can easily write down the interactions in terms of spin operators. If $\rho \ll 1$, we can just keep the nearest-neighbor-rung interactions because of fast decaying of the van der Waals interactions. Figure 2 shows the interactions between nearest-neighbor (NN) rungs, which contains the Rydberg interactions between atoms in the same leg $V_1 = V_0\rho^6$ and those between atoms in different legs $V_2 = V_0\rho^6 / (1 + \rho^2)^3$. The NN spin interactions are

$$\hat{H}_{2\text{LR,NN}} = \frac{V_1 - V_2}{2} \hat{L}_i^z \hat{L}_{i+1}^z + \frac{V_1 + V_2}{2} \left(\hat{L}_i^z \right)^2 \left(\hat{L}_{i+1}^z \right)^2. \quad (8)$$

For generic values of ρ , it is needed to include the long-range interactions. The interactions between the spin at site i and that at site $i+k$ takes the same form as Eq. (8) by replacing V_1, V_2 by $V_1^{(k)} = V_0\rho^6/k^6, V_2^{(k)} = V_0\rho^6 / (k^2 + \rho^2)^3$.

Finally, noticing that the Rydberg Rabi term can flip the spin projections between $|0\rangle$ and $|\pm 1\rangle$, but there is no direct flipping channel between $|+1\rangle$ and $|-1\rangle$, the Rabi term is equivalent to the spin-1 ladder operator. In summary, if the rung size of the two-leg ladder is smaller than the Rydberg blockade radius, or $V_0 \gg \Delta, \Omega$, the two-leg Rydberg ladder is an effective spin-1 chain

$$\begin{aligned} \hat{H}_{2\text{LR}}^{\text{eff}} = & -\Delta \sum_{i=1}^{N_s} \left(\hat{L}_i^z \right)^2 + \sum_k \left(\frac{V_1^{(k)} - V_2^{(k)}}{2} \sum_{i=1}^{N_s-k} \hat{L}_i^z \hat{L}_{i+k}^z \right. \\ & \left. + \frac{V_1^{(k)} + V_2^{(k)}}{2} \sum_{i=1}^{N_s-k} \left(\hat{L}_i^z \right)^2 \left(\hat{L}_{i+k}^z \right)^2 \right) \\ & + \frac{\Omega}{2} \sum_{i=1}^{N_s} \left(\hat{U}_i^+ + \hat{U}_i^- \right). \end{aligned} \quad (9)$$

We now consider the case where the long-range interactions have a negligible effect and keep only the NN interactions. In this situation the effective Hamiltonian reads

$$\begin{aligned} \hat{H}_{2\text{LR}}^{\text{eff}} = & -\Delta \sum_{i=1}^{N_s} \left(\hat{L}_i^z \right)^2 + \frac{V_1 - V_2}{2} \sum_{i=1}^{N_s-1} \hat{L}_i^z \hat{L}_{i+1}^z \\ & + \frac{V_1 + V_2}{2} \sum_{i=1}^{N_s-1} \left(\hat{L}_i^z \right)^2 \left(\hat{L}_{i+1}^z \right)^2 \\ & + \frac{\Omega}{2} \sum_{i=1}^{N_s} \left(\hat{U}_i^+ + \hat{U}_i^- \right). \end{aligned} \quad (10)$$

The matching with the target model requires

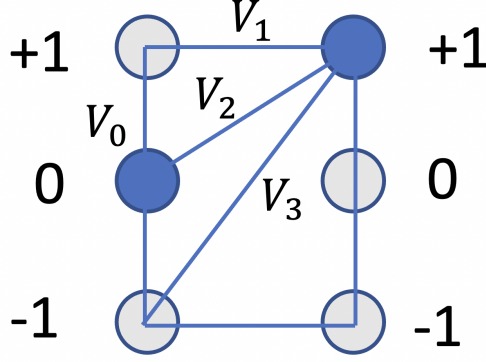


FIG. 3. The three-leg Rydberg ladder with $N_s = 2$ rungs. In each rung, the three states that have only one Rydberg state in the upper, middle, or lower leg are labeled by the spin $|+1\rangle$, $|0\rangle$, and $|-1\rangle$ states, respectively. In the same rung, the NN interaction is V_0 , and the NNN interaction is $V'_0 = V_0/64$. The inter-rung interactions between atoms in the same leg, in NN legs, and in NNN legs are V_1 , V_2 , and V_3 , respectively.

- $\Delta = -U/2$, note that the sign matters.
- The coefficient for $\hat{L}_i^z \hat{L}_{i+1}^z$ is positive for the simulator (repulsive/antiferromagnetic) but the CAHM has ferromagnetic interactions. This can be remedied by redefining the observable $\hat{L}_{2i+1}^z \rightarrow -\hat{L}_{2i+1}^z$ (staggered interpretation).
- After this redefinition $V_1 = -V_2 = Y > 0$ but $V_2 > 0$ with current technology.
- $\Omega = -X$, the sign does not matter because we can redefine the relative phase between $|g\rangle$ and $|r\rangle$ without physical consequences.

These results agree with two-rung results of [13].

B. Three-leg ladder

Another scheme to realize spin-one chains is to use a three-leg ladder, where the three states each with only one Rydberg state in a rung represent the three spin projection states in z direction [13]. The configuration is shown in Fig. 3, where five different types of interactions V_0 , V'_0 , V_1 , V_2 , and V_3 exist, and we allow a small offset for the detuning in the middle leg, $\Delta + \Delta_0$. There are eight states in a rung, four of which have more than one Rydberg states, and one of which has no Rydberg state. We consider two cases here.

In case 1, the whole rung is within the Rydberg blockade radius $2a_y < R_b$, only the four states with less than two Rydberg states are allowed in the low energy band. We can further tune the detuning Δ such that only the three states with one Rydberg state are allowed in the low-energy band. In case 1, we require $V_0, V'_0 \gg \Delta \gg |\Delta_0|, |\Omega|$.

In case 2, Rydberg states in NN legs in the same rung are blocked by letting $a_y < R_b$, but the size of the whole rung is larger than R_b , and the state with two Rydberg states in the upper and the lower legs in the same rung may has a lower energy than those states with one Rydberg state, that is $-2\Delta + V'_0 < -\Delta$ if $V'_0 = V_0/64 < \Delta$. Thus the spin-1 sector is not in the lowest energy band. If the energy gap $\Delta - V'_0 \gg \Omega$, the tunneling from the spin-1 sector to the ground state is small and the 3-leg Rydberg system can still simulate the spin-1 dynamics with good accuracy. In case 2, we require $V_0, \Delta, |V_0 - \Delta| \gg V'_0, |\Delta_0|, |\Omega|$.

For both cases, the three spin projection states are nearly degenerate and form an energy band that. They are nearly orthogonal to other Rydberg states. In both cases, in order to obtain the effective spin-1 Hamiltonian, we adapt the relation between the z -component of the spin-1 operator and the Rydberg number operator [13], proceed as in Eq. (6), impose the constraint that there is exactly one Rydberg state for the three spin-1 states, and obtain the equations

$$\begin{aligned}\hat{L}_i^z &= \hat{n}_{i,+1} - \hat{n}_{i,-1} \\ (\hat{L}_i^z)^2 &= \hat{n}_{i,+1} + \hat{n}_{i,-1} \\ \hat{n}_{i,-1} + \hat{n}_{i,0} + \hat{n}_{i,+1} &= 1\end{aligned}\tag{11}$$

When the detuning term is a uniform constant $-\Delta$, the constraint among the occupation numbers in a rung implies that the detuning energy is a constant. If we allow a small offset Δ_0 to the detuning in the middle leg [13], the detuning energy $\hat{H}_{detun.,i}$ at rung i reads

$$\hat{H}_{detun.,i} = \Delta_0 (\hat{L}_i^z)^2 - \Delta - \Delta_0.\tag{12}$$

The interaction term between NN rungs $\hat{H}_{3LR,NN}$ can be rewritten as

$$\begin{aligned}\hat{H}_{3LR,NN} &= [(3V_1 + V_3)/2 - 2V_2] (\hat{L}_i^z)^2 (\hat{L}_{i+1}^z)^2 \\ &+ [(V_1 - V_3)/2] \hat{L}_i^z \hat{L}_{i+1}^z \\ &+ (V_2 - V_1) \left[(\hat{L}_i^z)^2 + (\hat{L}_{i+1}^z)^2 \right] + V_1.\end{aligned}\tag{13}$$

The effective Hamiltonian for the Rabi term is different for the two cases mentioned above. In case 1, the whole rung is blockaded, the Rabi term can flip between each two of the three spin states via hopping back and forth between the empty state and the spin-1 sector. Notice that there also possibility for the atom jumping out from and going back to the same state, so the Rabi term effectively contributes both a diagonal term and a clock ladder operator \hat{C}_i^\pm which provides (anti)cyclic permutations.

In case 2, the energy of the $|rgr\rangle$ state is about $|\Delta|$ lower than the states in the spin-1 sector (V'_0 is small), while the energy of the empty state is the same amount higher. The hopping amplitudes of flipping between $|+1\rangle$ and $|-1\rangle$ via the empty state and that via the $|rgr\rangle$ state have the nearly the same magnitude but opposite signs so are canceled. The Rabi term is effectively a spin-1 ladder operator \hat{U}_i^\pm .

We can come to the same conclusion using perturbation theory to calculate the effective coupling constants. Treating the Rabi term as a perturbation, the effective Hamiltonian for the Rabi term is

$$\langle e' | \hat{H}_{3LR,\Omega}^{\text{eff}} | e \rangle = \frac{1}{2} \sum_{f \neq e, e'} \langle e' | \hat{H}_{3LR,\Omega} | f \rangle \langle f | \hat{H}_{3LR,\Omega} | e \rangle \left(\frac{1}{E_{e'} - E_f} - \frac{1}{E_f - E_e} \right), \quad (14)$$

where $|e\rangle(|f\rangle)$ is the state inside(outside) of the spin-1 sector. The effective matrix for the Rabi term in the spin-1 sector is

$$-\frac{\Omega^2}{4} \begin{pmatrix} A & \Gamma & \Lambda \\ \Gamma & B & \Gamma \\ \Lambda & \Gamma & A \end{pmatrix} \quad (15)$$

where

$$\begin{aligned} A &= \frac{1}{V_0 - \Delta - \Delta_0} + \frac{1}{V'_0 - \Delta} + \frac{1}{\Delta} \\ B &= \frac{2}{V_0 - \Delta} + \frac{1}{\Delta + \Delta_0} \\ 2\Gamma &= \frac{1}{\Delta} + \frac{1}{V_0 - \Delta} + \frac{1}{\Delta + \Delta_0} + \frac{1}{V_0 - \Delta - \Delta_0} \\ \Lambda &= \frac{1}{V'_0 - \Delta} + \frac{1}{\Delta} \end{aligned} \quad (16)$$

The diagonal part of the effective matrix can be written as $[(B - A)\Omega^2/4](\hat{L}_i^z)^2$ up to a constant. For case 1, $\Gamma \approx \Lambda \approx 1/\Delta$, the off-diagonal part is a three-state clock ladder

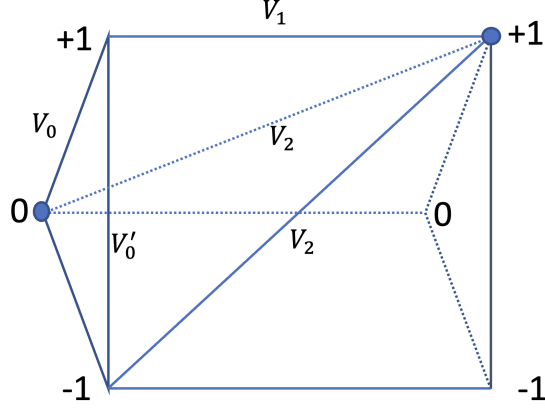


FIG. 4. Same as Fig. 3, but the middle leg is put out of plane to form a equilateral triangular prism.

operator. For case 2, $\Lambda \approx 0$, the off-diagonal part is a spin-1 ladder operator. Thus effectively

$$\hat{H}_{3\text{LR},\Omega}^{\text{eff}} = \begin{cases} -\frac{\Omega^2}{4\Delta} \sum_i (\hat{C}_i^+ + \hat{C}_i^-) & \text{for case 1,} \\ -\frac{\Omega^2\Gamma}{4} \sum_i (\hat{U}_i^+ + \hat{U}_i^-) & \text{for case 2.} \end{cases} \quad (17)$$

In summary, one can write down the effective spin-1 Hamiltonian for the three-leg Rydberg ladder

$$\begin{aligned} \hat{H}_{3\text{LR}}^{\text{eff}} &= \left[\Delta_0 + \frac{\Omega^2 (B - A)}{4} \right] \sum_{i=1}^{N_s} (\hat{L}_i^z)^2 \\ &+ (V_2 - V_1) \sum_{i=1}^{N_s-1} \left[(\hat{L}_i^z)^2 + (\hat{L}_{i+1}^z)^2 \right] \\ &+ \frac{V_1 - V_3}{2} \sum_{i=1}^{N_s-1} \hat{L}_i^z \hat{L}_{i+1}^z \\ &+ \left(\frac{3V_1 + V_3}{2} - 2V_2 \right) \sum_{i=1}^{N_s-1} (\hat{L}_i^z)^2 (\hat{L}_{i+1}^z)^2 \\ &+ \hat{H}_{3\text{LR},\Omega}^{\text{eff}} + \text{Const.} \hat{1}, \end{aligned} \quad (18)$$

where the constant $\text{Const.} = -(\Delta + \Delta_0)N_s - N_s\Omega^2B/4 + V_1(N_s - 1)$.

C. Triangular prism

If we allow the middle leg of the three-leg ladder moving out of plane, the effective Hamiltonian for case 1 does not change as long as the size of the whole rung is within R_b .

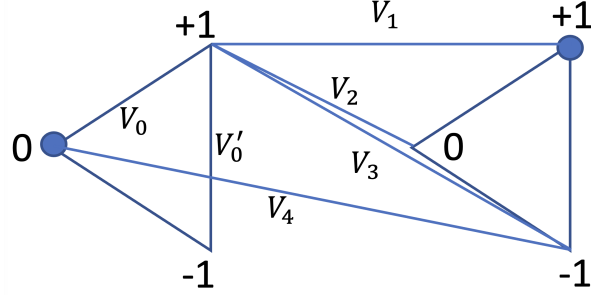


FIG. 5. Same as Fig. 4, but triangles reside in the same plane.

In particular, if the three sites in a rung form an equilateral triangle (Fig. 4), $V_2 = V_3$, and $V_0 = V_0' \gg \Delta \gg |\Delta_0|, |\Omega|$. Thus $\Gamma \approx \Lambda$, $B \approx A$, the effective Hamiltonian for the Rydberg simulator is

$$\begin{aligned}
\hat{H}_{\text{prism}}^{\text{eff}} &= \Delta_0 \sum_{i=1}^{N_s} (\hat{L}_i^z)^2 + (V_2 - V_1) \sum_{i=1}^{N_s-1} \left[(\hat{L}_i^z)^2 + (\hat{L}_{i+1}^z)^2 \right] \\
&+ \frac{V_1 - V_2}{2} \sum_{i=1}^{N_s-1} \hat{L}_i^z \hat{L}_{i+1}^z \\
&+ \frac{3(V_1 - V_2)}{2} \sum_{i=1}^{N_s-1} (\hat{L}_i^z)^2 (\hat{L}_{i+1}^z)^2 \\
&- \frac{\Omega^2 V_0}{4\Delta(V_0 - \Delta)} \sum_{i=1}^{N_s} (\hat{C}_i^+ + \hat{C}_i^-) + \text{Const.}\hat{I}.
\end{aligned} \tag{19}$$

Here, the coefficient of $\hat{L}_i^z \hat{L}_{i+1}^z$ and that of $(\hat{L}_i^z)^2 (\hat{L}_{i+1}^z)^2$ have fixed ratio, the physics originated from the competition between the two terms may be missing in the Hamiltonian. But the blockade radius required is just half of the one in Fig. 3.

D. Triangles in the same plane

As the three dimensional triangular prism is not easy to realize in experiment, we can just shift the middle leg in the same plane. As shown in Fig. 5, we shift the middle leg to left (or right). Now the off-rung interactions between nearest-neighbor legs depend on its

location and take two values V_2, V_4 . The effective Hamiltonian reads

$$\begin{aligned}
\hat{H}_{\text{in-plane}}^{\text{eff}} &= \Delta_0 \sum_{i=1}^{N_s} (\hat{L}_i^z)^2 \\
&+ \sum_{i=1}^{N_s-1} \left[(V_2 - V_1) (\hat{L}_i^z)^2 + (V_4 - V_1) (\hat{L}_{i+1}^z)^2 \right] \\
&+ \frac{V_1 - V_3}{2} \sum_{i=1}^{N_s-1} \hat{L}_i^z \hat{L}_{i+1}^z \\
&+ \left(\frac{3V_1 + V_3}{2} - V_2 - V_4 \right) \sum_{i=1}^{N_s-1} (\hat{L}_i^z)^2 (\hat{L}_{i+1}^z)^2 \\
&- \frac{\Omega^2 V_0}{4\Delta(V_0 - \Delta)} \sum_{i=1}^{N_s} (\hat{C}_i^+ + \hat{C}_i^-) + \text{Const.} \hat{\mathbb{I}}.
\end{aligned} \tag{20}$$

By shifting the middle leg, we have more degrees of freedom to tune the coefficients of the interaction terms: if V_0, Δ and Ω are fixed, we can tune Δ_0, a_x and the angle of the triangle to tune couplings of $(\hat{L}_i^z)^2, \hat{L}_i^z \hat{L}_{i+1}^z$, and $(\hat{L}_i^z)^2 (\hat{L}_{i+1}^z)^2$ terms.

III. NUMERICAL TESTS

We have derived the low-energy effective Hamiltonian for various Rydberg ladder systems using perturbation theory. All the effective spin-1 Hamiltonians obtained in Sec. II have the same form

$$\begin{aligned}
\hat{H}_{\text{eff}} &= D \sum_{i=1}^{N_s} (\hat{L}_i^z)^2 + R \sum_{i=1}^{N_s-1} \hat{L}_i^z \hat{L}_{i+1}^z \\
&+ R' \sum_{i=1}^{N_s-1} (\hat{L}_i^z)^2 (\hat{L}_{i+1}^z)^2 - J \sum_{i=1}^{N_s} (\hat{U}_i^+ + \hat{U}_i^-),
\end{aligned} \tag{21}$$

where the ladder operator \hat{U}_i^\pm can be replaced by the clock raising and lowering operator \hat{C}_i^\pm for the cases that allow hopping between $|\pm 1\rangle$ states. In this section, we provide some numerical calculations to test the validity of our results.

A. Two-leg ladder

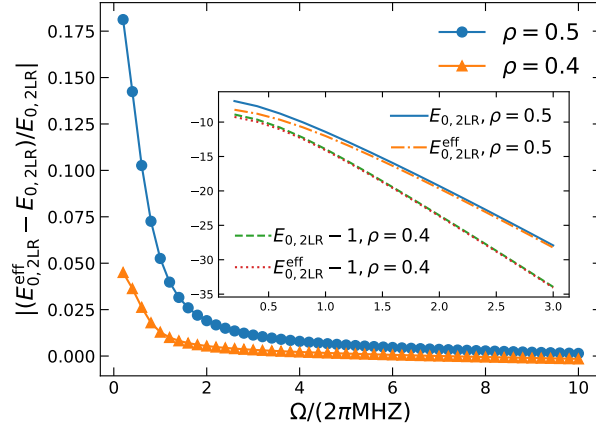


FIG. 6. The relative error of the ground-state energy $E_{0,2LR}^{\text{eff}}$ of the effective Hamiltonian (10) as a function of Ω . All the van der Waals interactions are kept in the original two-leg Rydberg ladder to compute the actual ground-state energy $E_{0,2LR}$. Here, $N_s = 16$, $V_0 = 1000 \times 2\pi$ MHz, $\Delta = 1 \times 2\pi$ MHz, and two inverse aspect ratios $\rho = 0.5, 0.4$ are considered. The inset shows the ground-state energy as a function of Ω . The energy for $\rho = 0.4$ is shifted by -1 for better view.

In this case, the effective Hamiltonian is shown in Eq. (10) with $D = -\Delta$, $R = (V_2 - V_1)/2$, $R' = (V_1 + V_2)/2$, $J = -\Omega/2$. Since the error of the effective Hamiltonian is of order $\Omega^2/(4V_0)$, we set V_0 to a large value. Given that $V_{ij} = C_6/r_{ij}^6$ with $C_6 = 858386 \times 2\pi$ MHz μm^6 , we set $V_0 = 1000 \times 2\pi$ MHz by taking the length of the rung to be $a_y = 3.083\mu\text{m}$. Figure 6 presents the ground-state energy difference between the two-leg Rydberg ladder \hat{H}_{2LR} and the corresponding effective Hamiltonian (10) as a function of Ω for $N_s = 16$, $\Delta = 1 \times 2\pi$ MHz. The effective Hamiltonian only contain NN interactions, while \hat{H}_{2LR} contains all van der Waals interactions. If the inverse aspect ratio $\rho = 0.5$, the relative energy difference is about 18% for small $\Omega = 0.2$, and decreases quickly toward zero as Ω is increased. For smaller inverse aspect ratio $\rho = 0.4$, the relative error behaves the same way but with an overall smaller magnitude. Note that the error from perturbation theory is of order $\Omega^2/(4V_0)$, which should increase as we increase Ω , but is small compared to the error from the omitted long-range interactions. For small Ω , the blockade radius $R_b/a_y = (V_0/\Omega)^{1/6}$ is large and the interactions beyond NN rungs play important roles and are not negligible. As we increase Ω , the blockade radius R_b is decreased and the effects of long-range interaction fade away.

By fixing a_y and increasing a_x such that ρ is decreased, R_b is becoming relatively smaller, so are the effects of long-range interaction. For $\Omega = 10$, $R_b \approx 2.154a_y$, slightly larger than $a_x = 2a_y$ for $\rho = 0.5$ and smaller than $a_x = 2.5a_y$ for $\rho = 0.4$. We conclude that it is safe to omit long-range interactions when the blockade radius R_b is small.

B. Three-leg ladder

We rewrite the Hamiltonian (18) with 00BC as

$$\begin{aligned} \hat{H}_{\text{eff1}} = & D \sum_{i=1}^{N_s} (\hat{L}_i^z)^2 + R \sum_{i=1}^{N_s-1} \hat{L}_i^z \hat{L}_{i+1}^z \\ & + R' \sum_{i=1}^{N_s-1} (\hat{L}_i^z)^2 (\hat{L}_{i+1}^z)^2 - J \sum_{i=1}^{N_s} (\hat{U}_i^+ + \hat{U}_i^-), \end{aligned} \quad (22)$$

where $D = \Delta_0 + J + 2(V_2 - V_1)$, $R = (V_3 - V_1)/2$, $R' = (V_3 + 3V_1)/2 - 2V_2$, $J = \Omega^2 V_0 / [4\Delta(V_0 - \Delta)]$. We can use exact diagonalization to show that the Rydberg system and the effective Hamiltonian have close energy density for small system sizes. But because the spin-1 sector is not the lowest energy band, we cannot check the effective Hamiltonian using normal DMRG which finds the ground state. We have seen that the effective Hamiltonian for triangular chain works well, so we believe Hamiltonian (22) well describe the physics of the spin-1 sector.

We can calculate time evolution of an initial state to check the effective Hamiltonian. In Fig. 7, we show the time evolution of the initial state $|0, 0, 0\rangle$ for $N_s = 3$, $V_0 = 2\Delta = 40 \times 2\pi \text{MHz}$, $\Omega = 2 \times 2\pi \text{MHz}$, $\rho = 1/3$. Three values of $\Delta_0/2\pi \text{MHz}$ are considered, 0, 0.2, 0.4, which corresponds to $(D, R, R', J) = (0.070261, -0.018332, 0.011408, 0.1)$, $(0.270261, -0.018332, 0.011408, 0.1)$, $(0.470261, -0.018332, 0.011408, 0.1)$

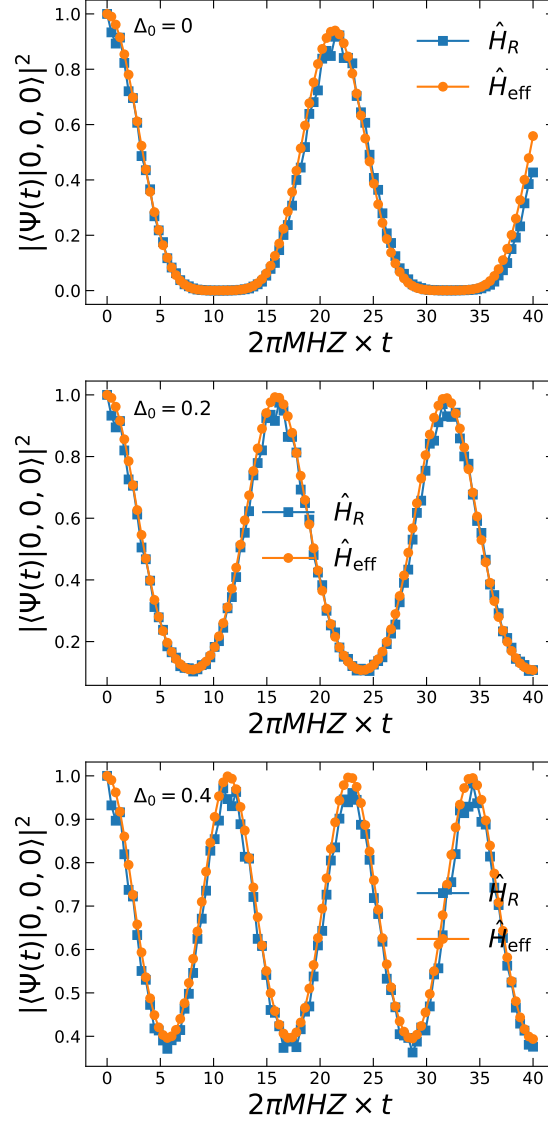


FIG. 7. Compare the real-time evolution of the initial state $|0, 0, 0\rangle$ with the Rydberg simulator to that with the effective Hamiltonian (22), $N_s = 3$, $\Delta_0 = (0, 0.2, 0.4)$, $V_0 = 2\Delta = 40$, $\Omega = 2$, $\rho = 1/3$. The parameters are in unit of $2\pi \text{MHz}$.

C. Equidistant equilateral triangles in plane

We have shown that the spin-1 effective Hamiltonians of the two-leg and three-leg Rydberg array have the same form

$$\begin{aligned}
\hat{H}_{S=1} = & D_1 (L_1^z)^2 + D \sum_{i=2}^{N_s-1} (\hat{L}_i^z)^2 + D_{N_s} (L_{N_s}^z)^2 \\
& + R \sum_{i=1}^{N_s-1} \hat{L}_i^z \hat{L}_{i+1}^z + R' \sum_{i=1}^{N_s-1} (\hat{L}_i^z)^2 (\hat{L}_{i+1}^z)^2 \\
& - J \sum_{i=1}^{N_s} (\hat{C}_i^+ + \hat{C}_i^-), \tag{23}
\end{aligned}$$

where $D = \Delta_0 + V_2 + V_4 - 2V_1$, $R = (V_3 - V_1)/2$, $R' = (V_3 + 3V_1)/2 - V_2 - V_4$, $J = \Omega^2 V_0 / [4\Delta(V_0 - \Delta)]$. We choose $D_1 = \Delta_0/2 + V_2 - V_1$ and $D_{N_s} = \Delta_0/2 + V_4 - V_1$ to minimize the boundary effects. Because if $D_1 = D_{N_s} = D$, the diagonal part has an energy $DN_s + R(N_s - 1) + R'(N_s - 1) = (D + R + R')N_s - R - R'$ for the ferromagnetic phase, which may have different signs for small and large system sizes. Calculations for small system may give wrong phase.

We compare the ground-state energy for the original Rydberg system and its effective Hamiltonian in Fig. 8. Notice that $V_2(\rho = 0.4) \approx 4$ and $V_2(\rho = 1/3) \approx 0.9$, the effective Hamiltonian well describe the low-energy physics for $V_0 = 2\Delta = 100 \times 2\pi$ MHz, $\Omega \leq 5 \times 2\pi$ MHz. Thus Hamiltonian (22) will also well describe the spin-1 sector for the three-leg ladder with $\rho \leq 0.5$.

For $\Delta_0 = 0$, $V_0 = 2\Delta = 100 \times 2\pi$ MHz, and $\rho = 0.4$, the values of (D, R, R') are $(3.26225434954982, -0.07359330845873141, -3.335847658008552)$. The phase transition can be characterized by the second-order Rényi entropy.

IV. PHASE DIAGRAMS

All the effective Hamiltonians for ladders have the same form

$$\begin{aligned}
\hat{H}_{\text{eff}} = & D \sum_{i=1}^L (\hat{L}_i^z)^2 + R \sum_{i=1}^{L-1} \hat{L}_i^z \hat{L}_{i+1}^z + R' \sum_{i=1}^{L-1} (\hat{L}_i^z)^2 (\hat{L}_{i+1}^z)^2 \\
& - J \sum_{i=1}^L (\hat{U}_i^+ + \hat{U}_i^-), \tag{24}
\end{aligned}$$

When D and R' are large positive, all spins are zero, which is the large- D phase. When R is large positive, the anti-ferromagnetic (AFM) phase is favored. When R is large negative,

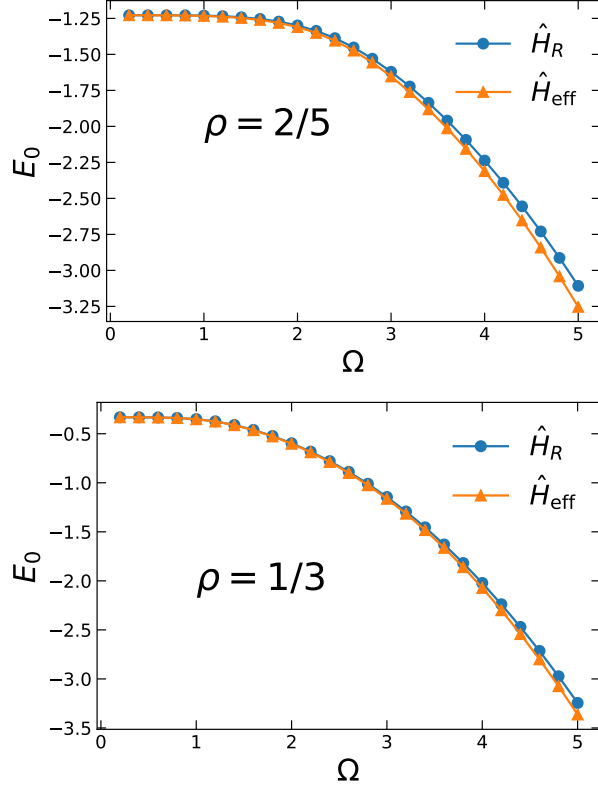


FIG. 8. Ground-state energy as a function of Ω for the Rydberg simulator and the effective Hamiltonian (23), $N_s = 8$, $\Delta_0 = 0$, $V_0 = 2\Delta = 100 \times 2\pi$ MHz, (top) $\rho = 0.4$, (bottom) $\rho = 1/3$.

the ferromagnetic (FM) phase is favored. The competition of the three diagonal terms may also favors the Rydberg state density wave (RDW) phase: the values of $\langle (\hat{L}_i^z)^2 \rangle$ are $1, 0, 1, 0, \dots$. The order parameters are $M_{\text{FM}} = 1/L \sum_i \hat{L}_i^z$, $M_{\text{AFM}} = 1/L \sum_i (-1)^i \hat{L}_i^z$, and $M_{\text{RDW}} = 1/L \sum_i (-1)^i (\hat{L}_i^z)^2$ for FM, AFM, and RDW, respectively.

A. Two-leg ladder: $a_x = 2a_y$

$$H_{2LR} = \frac{\Omega}{2} \sum_{i;s=1,2} (|g_{is}\rangle\langle r_{is}| + h.c.) - \Delta \sum_{i;s=1,2} \hat{n}_{i,s} \quad (25)$$

$$+ \sum_{is \neq i's'} V_{is,i's'} \hat{n}_{i,s} \hat{n}_{i',s'}. \quad (26)$$

Labeling the upper leg as spin $|+1\rangle$ state and the lower leg as spin $|-1\rangle$ state, $D = -\Delta$, $R = (V_1 - V_2)/2$, $R' = (V_1 + V_2)/2$, $J = -\Omega/2$. This corresponds to Eq. (10).

TABLE I. The values of order parameters for different phases. The corresponding susceptibilities diverge on the critical lines.

	M_{FM}	M_{AFM}	M_{RDW}
FM	$\neq 0$	$= 0$	$= 0$
AFM	$= 0$	$\neq 0$	$= 0$
FRDW	$\neq 0$	$\neq 0$	$\neq 0$
PRDW	$= 0$	$= 0$	$\neq 0$
Disorder	$= 0$	$= 0$	$= 0$

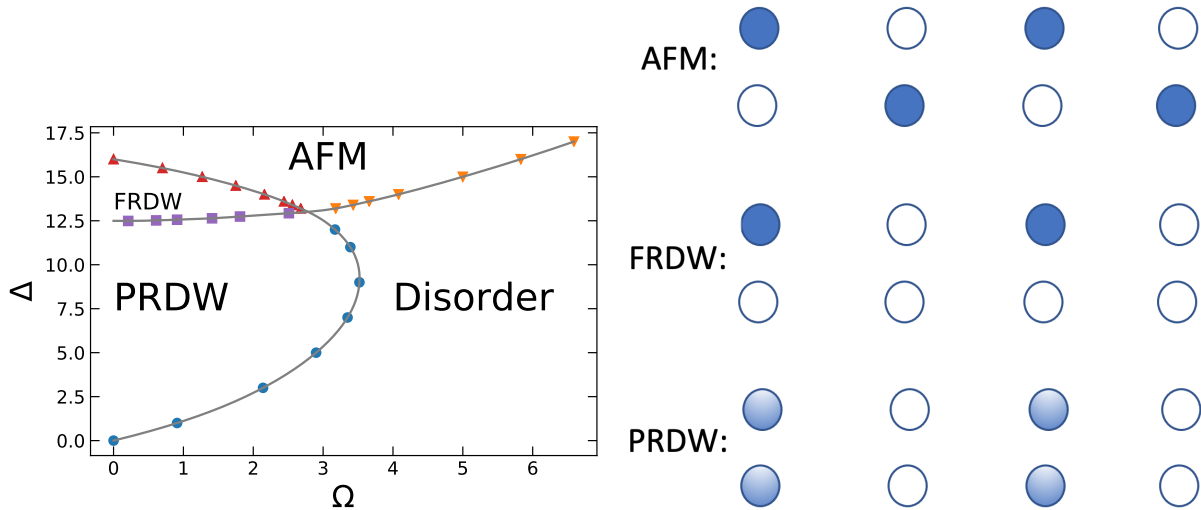


FIG. 9. Ground-state phase diagram for the effective Hamiltonian (22) of the two-leg Rydberg ladder. Here $L = 512$, $V_0 = 1000 \times 2\pi$ MHz, $\rho = a_y/a_x = 0.5$. The PRDW phase is disordered in even or odd sites, and the FRDW phase is FM in even or odd sites.

When $\Omega = 0$, the diagonal part of the Hamiltonian is in the Large- D phase for $\Delta < 0$, the RDW phase for $0 < \Delta < 2V_2$, and the AFM phase for $\Delta > 2V_2$. The RDW phase has high degeneracy with states $|\dots, \pm 1, 0, \pm 1, 0, \dots\rangle$. When Ω is turned on a little, the RDW phase splits into the ferromagnetic RDW (FRDW) phase ($|\dots, 1, 0, 1, 0, \dots\rangle$ or $|\dots, -1, 0, -1, 0, \dots\rangle$) and paramagnetic RDW (PRDW) phase ($\langle \hat{L}_i^z \rangle = 0$ but $\langle (\hat{L}_i^z)^2 \rangle = 1$ on even or odd sites). The critical line between FRDW and PRDW is an Ising critical line. One can perform degenerate perturbation theory for small Ω and obtain an effective Ising model on even or odd sites:

$$H_{\text{Ising}} = \frac{\Omega^2}{4} \left(-J_{\text{eff}} \sum_i \sigma_i^z \sigma_{i+2}^z - \frac{1}{\Delta} \sum_i \sigma_i^x \right). \quad (27)$$

with

$$J_{\text{eff}} = \left(\frac{1}{\Delta - V_1 - V_2} - \frac{1}{2\Delta - 4V_2} - \frac{1}{2\Delta - 4V_1} \right) \quad (28)$$

One can obtain the critical point between FRDW and PRDW in the $\Omega \rightarrow 0$ limit by equating the two coefficients. For large Ω , there may be quantum phase transitions between ordered phases and the disordered phase. Table I shows how to identify different phases using order parameters. The spin operators and the Rydberg state operators are related by Eqs. 6 and 6.

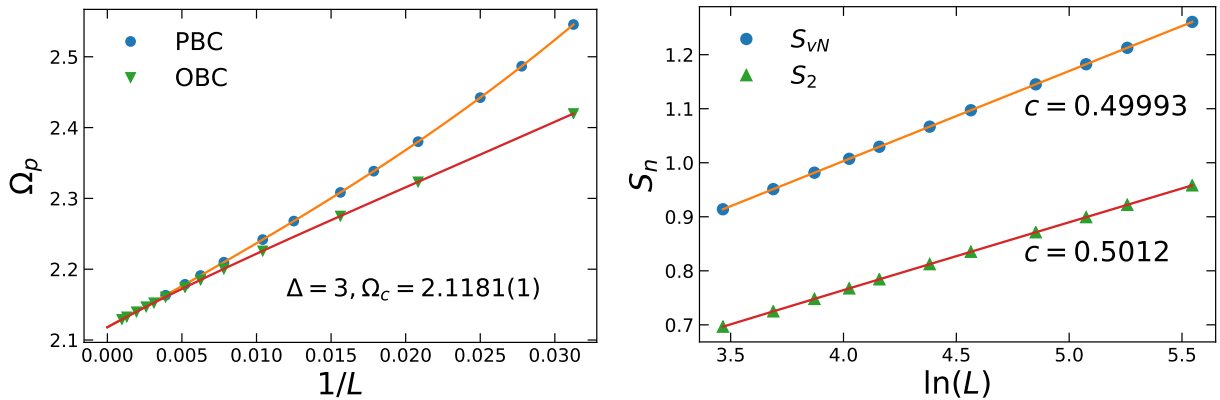


FIG. 10. Finite-size scaling of (top) the peak position of the PRDW susceptibility and (bottom) the first- and second-order Rényi entropy with PBC. The results are for the effective Hamiltonian (22) of the two-leg Rydberg ladder. Here $V_0 = 1000 \times 2\pi$ MHz, $\rho = 0.5$, $\Delta = 3$. The critical point separates the PRDW phase and the disordered phase, which belongs to the Ising universality class.

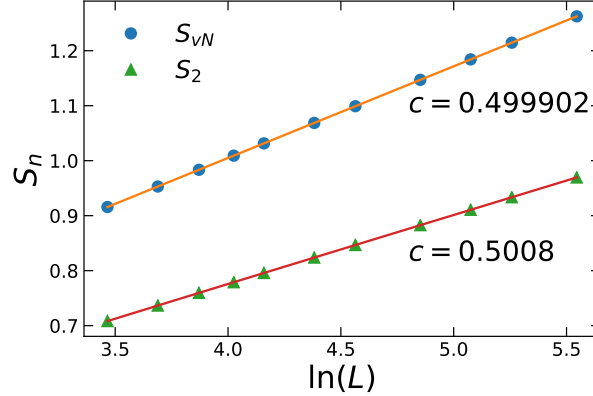


FIG. 11. Same as Fig. 10, but for $\Delta = 15, \Omega_c = 1.2531(1)$. The critical point separates FRDW phase and AFM phase, which is also in Ising universality class.

This suggest to study $\Delta > 0$ as an environment effect, staggered structures (cells with two sites) and to explore outside the region of validity of H_{eff} .

V. PRACTICAL APPLICATIONS

In this section, we discuss simple examples of real-time evolution for two leg ladders with 10 atoms (5 sites). This situation can be implemented remotely using QuEra facilities or simulated with a local SDK [8, 22]. In this case, the system is initialized with the 10 atoms in the ground state. This initial state is invariant under the transformation $\hat{L}_i^z \rightarrow -\hat{L}_i^z$ or equivalently swapping the two legs of the ladder and as we turn on the evolution the $\langle \hat{L}_i^z \rangle$ remain zero. For this reason, we display the values of $\langle (L_i^z)^2 \rangle$ for the five sites which is also invariant under staggered redefinitions of \hat{L}_i^z . Note also that the results are left-right symmetric. Results for the typical QuEra values $\Omega = 4\pi MHz$, $\Delta = 2\Omega$, $\rho = 0.5$ and the distance between the sites $a_x = 1R_b \simeq 8.7\mu m$ are shown below. The distance between the two atoms on one site is $a_y = 0.5R_b$ so $|rr\rangle$ at that site are unlikely. The evolution for a period $0.5 \mu s$ is shown in Fig. 12, with exact diagonalization for the 10 site problem, the QuEra local simulator and the effective Hamiltonian. It appears clearly that the three methods give very similar results. A finer comparison for the first three sites in Fig. 13 confirms that the effective Hamiltonian results are in excellent agreement.

We have also explored values of the parameters that are slightly outside the range of validity of H_{eff} . As a first example we keep $\rho = 0.5$, but we reduce the lattice spacing

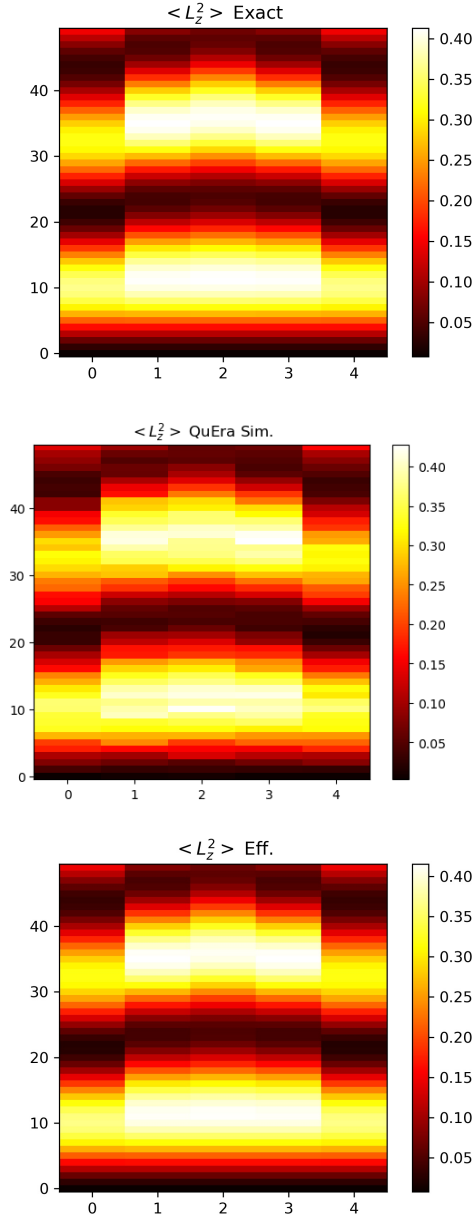


FIG. 12. Values of $\langle (\hat{L}_i^z)^2 \rangle$ for five sites, $\Omega = 4\pi$ MHz, $\Delta = 2\Omega$, $\rho = 0.5$ $a_x = 1R_b$ and $a_y = 0.5 \times R_b$. The vertical time units are 10^{-8} s. Top: exact diagonalization. Middle: QuEra (local simulator). Bottom: Effective Hamiltonian.

to $a_x = R_b/2$. The bloquade mechanism is even more effective but $a_x = R_b/2$ implies next to nearest neighbor interactions not taken into account in the simple $H_{eff.}$ with just NN interactions as in Eq. (10). Fig. 14 makes clear that the effective description is a less accurate description of the simulator than in the previous case, however, there is a qualitative

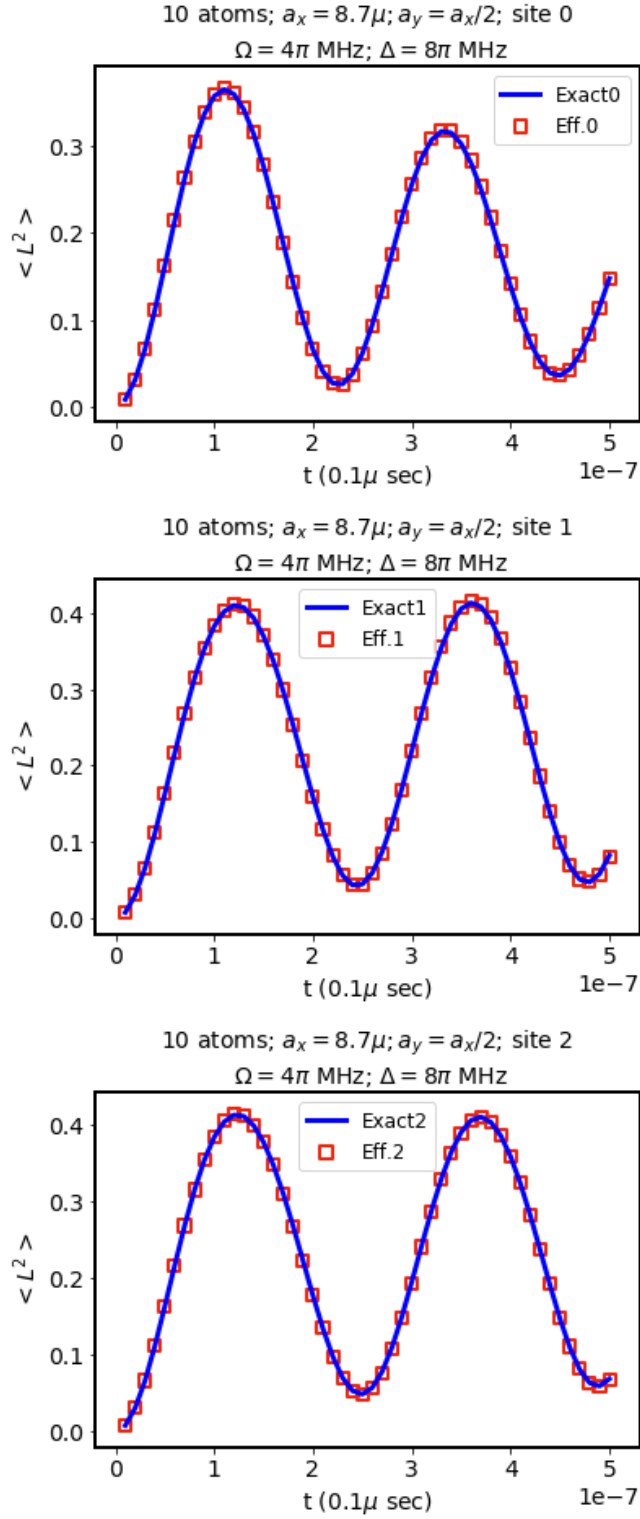


FIG. 13. Values of $\langle (\hat{L}_i^z)^2 \rangle$ for the first three of the five sites.

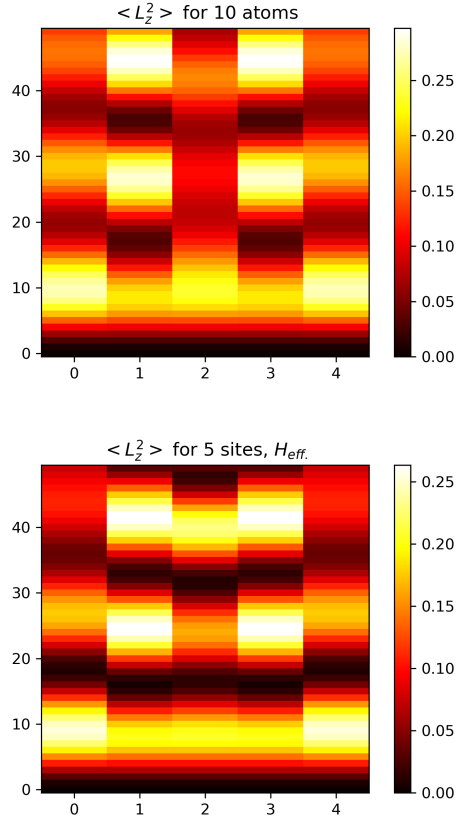


FIG. 14. 5 sites, $\rho = 0.5$, $a_x = 0.5 \times R_b$, $\Omega = 4\pi\text{MHz}$, $\Delta = 2\Omega$, vertical time units are $0.01\mu\text{sec}$. Top: 10 atom simulator. Bottom: 5 site H_{eff} .

agreement between the exact diagonalization with 10 atoms and the corresponding H_{eff} . It should also be noticed that for $a_x = R_b/2$, V_1 and V_2 are 64 times larger than in the previous case and the quartic term becomes very important. This is signaled by $L_z = 0$ bands screening the electric field both in the effective theory and the original simulator. This is illustrated in Fig. 15.

The screening effect observed in the previous deformation can be partially remediated by rather increasing ρ in order to have $V_2 \ll V_1$. For this reason we considered the case $\rho = 2$, $a_x = R_b$. The results are shown in Fig. 16.

VI. CONCLUSION

In summary we have considered ladder-shaped Rydberg arrays with two or three atoms per site. Originally these simulators were designed with the idea of mimicing closely the

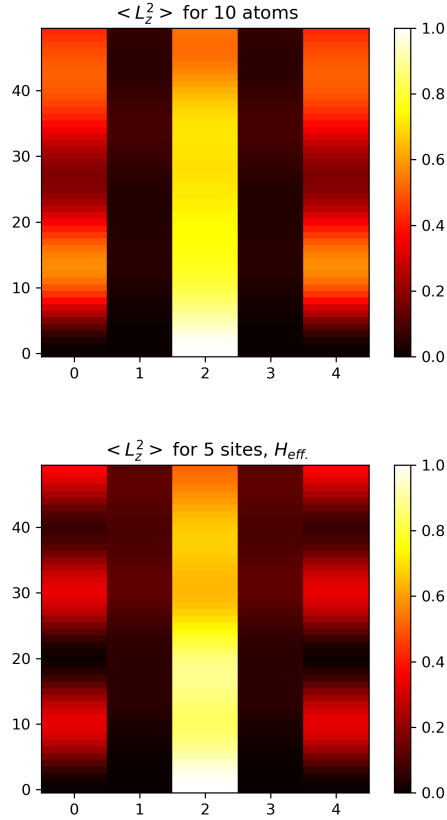


FIG. 15. 5 sites, $\rho = 0.5$, $a_x = 0.5 \times R_b$, $\Omega = 4\pi\text{MHz}$, $\Delta = 2\Omega$, vertical time units are $0.01\mu\text{sec}$. Top: 10 atom simulator. Bottom: 5 site H_{eff} .

evolution of the compact Abelian Higgs model. We constructed an effective Hamiltonian valid when the size of the rungs is small enough and the distance between the rungs not too small. In all cases, we found that the effective Hamiltonians have the same three types of terms as the target model plus an extra quartic term. The effect of the extra term is significant at positive detuning and is responsible for new quantum phases. More generally, the ladder models have a very rich phase diagram that is currently being explored using QuEra [8]. Matching the effective theory with the target gauge theory requires $\Delta < 0$ (cost for producing electric field). The new phases appear when $\Delta > 0$ ($m = \pm 1$ form the degenerate ground state). It is possible that a positive detuning could be used as an environment effect relevant in the context of hybrid hadronization [15]. Potential issue with microscopic string breaking generated by extra terms with a large coefficient suggest to study staggered structures (cells with two sites) that could be used to describe models different

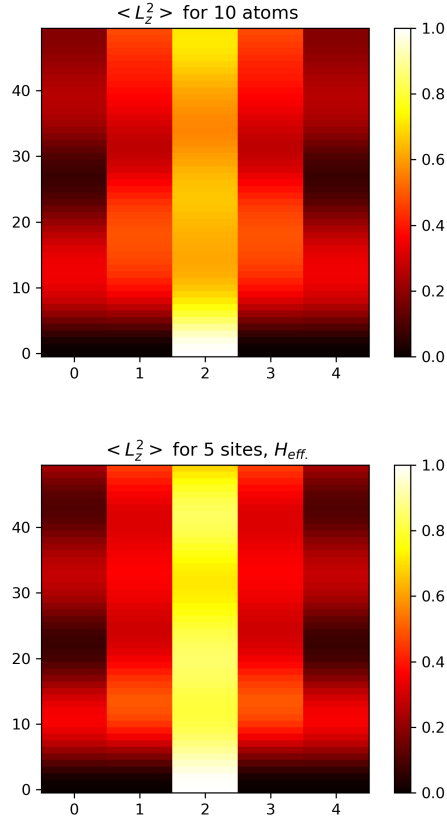


FIG. 16. 5 sites, $\rho = 2$, $a_x = 1 \times R_b$, $\Omega = 4\pi\text{MHz}$, $\Delta = 2\Omega$, vertical time units are $0.01\mu\text{sec}$. Top: 10 atom simulator. Bottom: 5 site H_{eff} .

from the target CAHM.

It should also be noted that there has been interest in inhomogeneous phases and the Lifshitz regime for QCD at finite temperature and density [23]. It has been argued that [24] that for massless quarks in the large N_c limit, dimensional reduction occurs and “chiral spiral” condensates appear [25]. In this scenario, the chiral spiral phase could appear at the end of the crossover line and separate an ordered phase where chiral symmetry is restored from the hadronic (confining) phase where chiral symmetry is broken (see Fig. 6 in [23]). In this context, exploring the possibility of inhomogeneous phase in simulators is an interesting direction of research.

In the future, it would also be interesting to have a simulator where negative (attractive) couplings among atoms could be engineered. This would allow us to cancel the extra terms and to have an effective Hamiltonian identical to the target Hamiltonian. Similar

technological needs to be present for quantum simulation of the tricritical Ising model (with different types of NNN interactions being negative) [14]. As we are moving toward better local control of the individual atoms we should look forward to using new technologies for lattice gauge theory. It would also be interesting to compare the manipulation of the three states associated with a rung in our approach with qutrit simulations [26, 27] and figure out if the extra quartic term found here could be understood in the context of Symanzik improvement [28, 29]

ACKNOWLEDGMENTS

We thank Sergio Cantu, James Corona, Fangli Liu, Kenny Heitritter, Steve Mrenna, Shengtao Wang and members of QuLAT for helpful discussions. This work was supported in part by the National Science Foundation (NSF) RAISE-TAQS under Award Number 1839153 (SWT). Computations were performed using the computer clusters and data storage resources of the HPCCC, which were funded by grants from NSF (MRI-1429826) and NIH (1S10OD016290-01A1). Y.M. is supported in part by the Dept. of Energy under Award Number DE-SC0019139. J.Z. is supported by NSFC under Grants No. 12304172 and No. 12147102, Chongqing Natural Science Foundation under Grant No. CSTB2023NSCQ-MSX0048, and Fundamental Research Funds for the Central Universities under Projects No. 2023CDJXY-048 and No. 2020CDJQY-Z003. Y. M. thanks the Amazon Web Services and S. Hassinger for facilitating remote access to QuEra through the Amazon Braket.

-
- [1] M. Dalmonte and S. Montangero, *Contemp. Phys.* **57**, 388 (2016), arXiv:1602.03776 [cond-mat.quant-gas].
 - [2] M. C. Bañuls *et al.*, *Eur. Phys. J. D* **74**, 165 (2020), arXiv:1911.00003 [quant-ph].
 - [3] V. Kasper, G. Juzeliunas, M. Lewenstein, F. Jendrzejewski, and E. Zohar, *New J. Phys.* **22**, 103027 (2020), arXiv:2006.01258 [quant-ph].
 - [4] C. W. Bauer *et al.*, *PRX Quantum* **4**, 027001 (2023), arXiv:2204.03381 [quant-ph].
 - [5] H. Bernien, S. Schwartz, A. Keesling, H. Levine, A. Omran, H. Pichler, S. Choi, A. S. Zibrov, M. Endres, M. Greiner, V. Vuletić, and M. D. Lukin, *Nature (London)* **551**, 579 (2017), arXiv:1707.04344 [quant-ph].

- [6] A. Keesling *et al.*, *Nature* **568**, 207 (2019), arXiv:1809.05540 [quant-ph].
- [7] A. Browaeys and T. Lahaye, *Nature Phys.* **16**, 132 (2020).
- [8] “Quera,” <https://www.quera.com>.
- [9] “Pasqal,” <https://www.pasqal.com>.
- [10] A. Celi, B. Vermersch, O. Viyuela, H. Pichler, M. D. Lukin, and P. Zoller, *Phys. Rev. X* **10**, 021057 (2020), arXiv:1907.03311 [quant-ph].
- [11] F. M. Surace, P. P. Mazza, G. Giudici, A. Lerose, A. Gambassi, and M. Dalmonte, *Phys. Rev. X* **10**, 021041 (2020), arXiv:1902.09551 [cond-mat.quant-gas].
- [12] S. Notarnicola, M. Collura, and S. Montangero, *Phys. Rev. Res.* **2**, 013288 (2020), arXiv:1907.12579 [cond-mat.quant-gas].
- [13] Y. Meurice, *Phys. Rev. D* **104**, 094513 (2021), arXiv:2107.11366 [quant-ph].
- [14] K. Slagle, D. Aasen, H. Pichler, R. S. K. Mong, P. Fendley, X. Chen, M. Endres, and J. Alicea, *Phys. Rev. B* **104**, 235109 (2021), arXiv:2108.09309 [cond-mat.str-el].
- [15] K. Heitritter, Y. Meurice, and S. Mrenna, (2022), arXiv:2212.02476 [quant-ph].
- [16] A. Bazavov, Y. Meurice, S.-W. Tsai, J. Unmuth-Yockey, and J. Zhang, *Phys. Rev.* **D92**, 076003 (2015), arXiv:1503.08354 [hep-lat].
- [17] Y. Kuno, S. Sakane, K. Kasamatsu, I. Ichinose, and T. Matsui, *Phys. Rev. D* **95**, 094507 (2017), arXiv:1605.00333 [cond-mat.quant-gas].
- [18] D. González-Cuadra, E. Zohar, and J. I. Cirac, *New J. Phys.* **19**, 063038 (2017), arXiv:1702.05492 [quant-ph].
- [19] J. Zhang, J. Unmuth-Yockey, J. Zeiher, A. Bazavov, S. W. Tsai, and Y. Meurice, *Phys. Rev. Lett.* **121**, 223201 (2018), arXiv:1803.11166 [hep-lat].
- [20] T. Chanda, M. Lewenstein, J. Zakrzewski, and L. Tagliacozzo, *Phys. Rev. Lett.* **128**, 090601 (2022), arXiv:2107.11656 [hep-th].
- [21] N. Šibalić and C. S. Adams, *Rydberg Physics*, 2399-2891 (IOP Publishing, 2018).
- [22] “Amazon braket,” <https://aws.amazon.com/braket>.
- [23] R. D. Pisarski, V. V. Skokov, and A. M. Tsvelik, *Universe* **5**, 48 (2019), arXiv:2202.01036 [hep-ph].
- [24] T. Kojo, Y. Hidaka, L. McLerran, and R. D. Pisarski, *Nucl. Phys. A* **843**, 37 (2010), arXiv:0912.3800 [hep-ph].
- [25] G. Basar and G. V. Dunne, *Phys. Rev. Lett.* **100**, 200404 (2008), arXiv:0803.1501 [hep-th].

- [26] E. Gustafson, Phys. Rev. D **103**, 114505 (2021), arXiv:2104.10136 [quant-ph].
- [27] E. Gustafson, (2022), arXiv:2201.04546 [quant-ph].
- [28] M. Carena, H. Lamm, Y.-Y. Li, and W. Liu, Phys. Rev. Lett. **129**, 051601 (2022), arXiv:2203.02823 [hep-lat].
- [29] M. Carena, E. J. Gustafson, H. Lamm, Y.-Y. Li, and W. Liu, Phys. Rev. D **106**, 114504 (2022), arXiv:2208.10417 [hep-lat].
- [30] J. Unmuth-Yockey, J. Zhang, A. Bazavov, Y. Meurice, and S.-W. Tsai, Phys. Rev. D **98**, 094511 (2018).
- [31] J. Zhang, Y. Meurice, and S.-W. Tsai, Phys. Rev. B **103**, 245137 (2021).

Appendix: Compact scalar QED

Matching the matrix elements to the target model $H_{eff} = \hat{H}_F + Const.\hat{I}$ ($Const.$ is a constant), we have the following equations for OBC

$$\begin{aligned} Const. &= -\Delta - \Delta_0 + \frac{\Omega^2}{4} \left(\frac{2}{\Delta - V_0} - \frac{1}{\Delta} \right) \\ \frac{U}{2} &= \Delta_0 + \frac{\Omega^2 V_0}{4\Delta(V_0 - \Delta)} \\ X &= \frac{\Omega^2 V_0}{2\Delta(V_0 - \Delta)} \end{aligned} \quad (A.1)$$

For 00BC,

$$\begin{aligned} Const. &= -\Delta - \Delta_0 + 2V_1 + \frac{\Omega^2}{4} \left(\frac{2}{\Delta - V_0} - \frac{1}{\Delta} \right) \\ \frac{U}{2} + Y &= \Delta_0 + 2(V_2 - V_1) + \frac{\Omega^2 V_0}{4\Delta(V_0 - \Delta)} \\ X &= \frac{\Omega^2 V_0}{2\Delta(V_0 - \Delta)} \end{aligned} \quad (A.2)$$

We can perform the same procedure for two rungs. The configurations are shown in Fig. 3. We obtain the following equations for 00BC

$$\begin{aligned} Const. &= -(\Delta + \Delta_0)N_s + (N_s + 1)V_1 \\ &\quad + \frac{\Omega^2}{4} \left(\frac{2}{\Delta - V_0} - \frac{1}{\Delta} \right) N_s \\ U &= 2\Delta_0 + 2V_3 - 2V_1 + \frac{\Omega^2 V_0}{2\Delta(V_0 - \Delta)} \\ Y &= 2V_2 - V_1 - V_3 \\ 2(Y + Y') &= V_1 - V_3 \\ X &= \frac{\Omega^2 V_0}{2\Delta(V_0 - \Delta)} \end{aligned} \quad (A.3)$$

$$(A.4)$$

Notice that it is impossible to match the boundary terms for OBC, which requires $V_1 = V_3$. Now we can tune the parameters in Rydberg systems to obtain the target model Eq. (A.7). For example, the target model with $U = 0, X = 0.02, Y/X = 0.35, Y'/X = 12.627$ corresponds to $V_0/\Delta = 2, V_0/\Omega = 100, \Delta_0/\Omega = 0.509, \rho = a_y/a_x = 0.431$ in the Rydberg simulator.

We have freedom to change the ratio V_0/Δ to match the same point. The lowest two energy densities are $(-0.01017156, -0.00357107, N_s = 2), (-0.00995229, -0.00619866,$

$N_s = 3$), $(-0.00983596, -0.00730903, N_s = 4)$ for the target model and $(-0.00998068, -0.00338451, N_s = 2)$, $(-0.00976367, -0.00599897, N_s = 3)$, $(-0.009649, -0.00710675, N_s = 4)$ for the Rydberg simulator. The errors are all of order 10^{-4} , consistent with the perturbation theory.

Matching to the target Hamiltonian (A.7), $U = -2\Delta + 2V_2$, $Y = -V_2$, $Y' = (V_1 + V_2)/2$. We can only simulate negative Y using this two-leg Rydberg ladder. The errors of the effective Hamiltonian are from the transition from the spin-1 sector to the $|rr\rangle$ state, which is of order $\Omega^2/(4V_0)$, and from the next-nearest-neighbor interactions $\sim V_1/64$.

The model is the Lattice scalar QED (sQED) on a $N_s \times N_\tau$ Euclidean spacetime lattice. There are two more columns on two sides, the 0th and the (N_s+1) th columns, controlling the boundary conditions. We use 00 boundary condition (00BC), where the plaquette (field) quantum numbers on the 0th and the $(N_s + 1)$ th columns are zero thus the total charge in the system is zero. In the time continuum limit [16, 30], we obtain the Hamiltonian in the charge representation

$$\begin{aligned} \hat{H}_C = & \frac{U}{2} \sum_{1 \leq j, k \leq N_s} c_{jk} S_j^z S_k^z + \frac{Y}{2} \sum_{i=1}^{N_s+1} (S_i^z)^2 \\ & - \frac{X}{2} \sum_{i=1}^{N_s} (\hat{U}_i^+ \hat{U}_{i+1}^- + \hat{U}_i^- \hat{U}_{i+1}^+) , \sum_i S_i^z = 0 \end{aligned} \quad (\text{A.5})$$

where $c_{jk} = N_s + 1 - \max\{j, k\}$. The eigenvalues of the operator S^z ($S^z|n\rangle = n|n\rangle$) are integer charge $n = 0, \pm 1, \pm 2, \dots$ attached on the vertical links, and the eigenstates define basis of the charge representation. The operator \hat{U}^\pm raises (lowers) the charge of a state by one $\hat{U}^\pm|n\rangle = |n \pm 1\rangle$. When the gauge coupling $U = 0$, the spin-1 truncation has an infinite-order phase transition from a gapped phase into a BKT critical line [31]. For nonzero gauge coupling, Eq. (A.5) has unusual long-range interactions, thus it is difficult to design quantum simulators for it. Using Gauss's Law, we can go to the field representation

$$\begin{aligned} \hat{H}_F = & \frac{U}{2} \sum_{p=1}^{N_s} (L_p^z)^2 + \frac{Y}{2} \sum_{p=1}^{N_s+1} (L_p^z - L_{p-1}^z)^2 \\ & - \frac{X}{2} \sum_{p=1}^{N_s} (U_p^+ + U_p^-) , \end{aligned} \quad (\text{A.6})$$

where the eigenvalues of L^z is the field quantum numbers $m = 0, \pm 1, \pm 2, \dots$ attached to the plaquettes. There are N_s plaquettes and $N_s + 1$ links, $L_0^z = L_{N_s+1}^z = 0$ under 00BC. For open boundary conditions (OBCs), p is taken from 2 to N_s , the Hamiltonian contains multiple charge sectors that have total charge $L_{N_s}^z - L_1^z$.

The field representation is identical to the charge representation without applying a truncation. The two Hamiltonians are quite different for small spin truncations. For one plaquette with two links, the basis in the field representation is $| -S \rangle, | -S + 1 \rangle, \dots, | S \rangle$. The basis in the charge representation is $| -S, S \rangle, | -S + 1, S - 1 \rangle, \dots, | S, -S \rangle$. The two Hilbert spaces observe one-to-one mapping. But for two plaquettes with three links, the dimensions of the two Hilbert spaces are not the same, e.g. for $S = 1$, the basis in the field representation is $| -1, -1 \rangle, | -1, 0 \rangle, | -1, 1 \rangle, | 0, -1 \rangle, | 0, 0 \rangle, | 0, 1 \rangle, | 1, -1 \rangle, | 1, 0 \rangle, | 1, 1 \rangle$, the corresponding states that satisfy Gauss's law in the charge representation are $| -1, 0, 1 \rangle, | -1, 1, 0 \rangle, | -1, 2, -1 \rangle, | 0, -1, 1 \rangle, | 0, 0, 0 \rangle, | 0, 1, -1 \rangle, | 1, -2, 1 \rangle, | 1, -1, 0 \rangle, | 1, 0, -1 \rangle$. The two states $| -1, 2, -1 \rangle, | 1, -2, 1 \rangle$ are truncated in the charge representation with spin-1 truncation. Generally, for N_s plaquettes with $N_s + 1$ links, if the states $| m_1, m_2, \dots, m_L \rangle$ with $| m_p - m_{p+1} | > S$ in the field representation have large energy gap to other states, the effective low-energy basis is a subset of basis in the charge representation with the same spin truncation.

For spin-1 truncation, we can add a high energy penalty for states $| \dots, \pm 1, \mp 1, \dots \rangle$. We have a new Hamiltonian

$$\hat{H}_F = \frac{U}{2} \sum_{p=1}^{N_s} (L_p^z)^2 + \frac{Y}{2} \sum_{p=1}^{N_s+1} (L_p^z - L_{p-1}^z)^2 \quad (\text{A.7})$$

$$\begin{aligned} & - \frac{Y'}{2} \sum_{p=1}^{N_s+1} L_p^z L_{p-1}^z (L_p^z - L_{p-1}^z)^2 - \frac{X}{2} \sum_{p=1}^{N_s} (U_p^+ + U_p^-) \\ & = \left(\frac{U}{2} + Y \right) \sum_{p=1}^{N_s} (L_p^z)^2 - (Y + Y') \sum_{p=1}^{N_s+1} L_p^z L_{p-1}^z \\ & + Y' \sum_{p=1}^{N_s+1} (L_p^z)^2 (L_{p-1}^z)^2 - \frac{X}{2} \sum_{p=1}^{N_s} (U_p^+ + U_p^-), \end{aligned} \quad (\text{A.8})$$

where the Y' term is only nonzero for states $| \dots, \pm 1, \mp 1, \dots \rangle$. For OBC, the coefficients of $(\hat{L}_p^z)^2$ at $p = 1, N_s$ are $U/2 + Y/2$ instead of $U/2 + Y$. The energy gap in the field representation will be closer to that in the charge representation by setting $Y' \gg 1$. The states in the charge representation like $| \dots, 111, \dots \rangle$ are not in the basis of the field representation, so the field representation with spin-1 truncation has no infinite-order phase transitions, either. But it has other interesting critical points and we are interested in quantum simulation of Eq. (A.7) using Rydberg ladders. The raising and lowering operators U^\pm can be replaced by clock matrices C^\pm which have additional element connecting -1 and 1 . The same idea can be applied to higher spin truncation to approach the true sQED.

For 00BC, $\hat{H}_{\text{eff}} \rightarrow \hat{H}_{\text{eff}} + (V_2 - V_1)[(L_1^z)^2 + (L_{N_s}^z)^2] + 2V_1 \hat{I}$. Notice that one can tune

the first and the last Δ_0 locally to realize 00BC, so we do not really need to add two more Rydberg atoms. This method can be generalized to arbitrary spin truncation, where $2S + 1$ legs are needed for spin- S truncation. But there is a simpler configuration to realize spin-1 truncation: the two-leg ladder.

The equations relating the parameters for 00BC are

$$\begin{aligned}
Const. &= -(\Delta + \Delta_0)N_s + (N_s + 1)V_1 + \frac{\Omega^2}{4} \left(\frac{2}{\Delta - V_0} - \frac{1}{\Delta} \right) N_s \\
U &= 2\Delta_0 + 2V_2 - 2V_1 \\
Y &= V_2 - V_1 \\
Y' &= -\frac{3}{2}Y \\
X &= \frac{\Omega^2 V_0}{2\Delta(V_0 - \Delta)}.
\end{aligned} \tag{A.9}$$

In this case, the Rydberg simulator can only simulate the target model with negative Y and fixed ratio $Y'/Y = -3/2$.

$$\begin{aligned}
\hat{H}_{Fc} &= \left(\frac{U}{2} + Y \right) \sum_{p=1}^{N_s} (L_p^z)^2 + \frac{Y}{2} \sum_{p=1}^{N_s+1} L_p^z L_{p-1}^z \\
&\quad - \frac{3Y}{2} \sum_{p=1}^{N_s+1} (L_p^z)^2 (L_{p-1}^z)^2 - \frac{X}{2} \sum_{p=1}^{N_s} (\hat{C}_p^+ + \hat{C}_p^-),
\end{aligned} \tag{A.10}$$